OCT Angiography

Eun Ji Lee

Abstract

Optical coherence tomography angiography (OCTA) is a relatively new technology that enables noninvasive visualization of the microvasculature of ocular tissues. Altered ocular perfusion being understood as an important factor in the pathogenesis of glaucoma, OCTA has emerged as a promising tool to evaluate ocular blood flow in patients with glaucoma. OCTA may have the potential to provide new information about the pathophysiology of glaucoma, as well as to assist in its diagnosis and treatment. This chapter briefly describes the basic principles and interpretation of OCTA, and evaluates its clinical use in patients with glaucoma. This chapter also introduces recent research findings observed using OCTA in glaucoma, including microvascular changes in the optic nerve head, retina, and choroid, and discusses how they may be related to the pathophysiology of glaucoma.

Keywords

OCT angiography · Ocular perfusion
Glaucoma · Microvasculature · Optic nerve head · Retina · Choroid

E. J. Lee (✉)
Seoul National University Bundang Hospital, Seongnam, Korea
e-mail: opticdisc@snubh.org

1 Introduction

Alterations in ocular perfusion have long been implicated in the pathogenesis of glaucoma. Compromised ocular blood flow (Huber et al. 2004; Findl et al. 2000; Shiga et al. 2016; Sehi et al. 2014) and reduced perfusion of the retina and choroid (Schwartz et al. 1977; Hitchings and Spaeth 1977; Yamazaki et al. 1996; Laatikainen 1971; O'Brart et al. 1997; Funaki et al. 1997) have been associated with glaucoma. Epidemiologic and clinical studies have demonstrated associations between glaucoma and low blood pressure (Tielsch et al. 1995; Bonomi et al. 2000; Leske et al. 1995) and nocturnal reductions in blood pressure (Graham and Drance 1999; Charlson et al. 2014). However, details of the role of ocular perfusion in glaucoma have remained elusive due to limitations in methods used to assess ocular blood flow.

Optical coherence tomography (OCT) angiography (OCTA) is a new imaging technique that enables visualization of the retinal and choroidal microvasculature, producing a three-dimensional (3D) reconstruction of vascular networks. OCTA providing structural and vascular maps in tandem, it is considered a promising tool to evaluate ocular perfusion in individual structural layers. Moreover, OCTA is noninvasive and does not require injection of dye, making it free from adverse effects and enabling repeated performance in busy clinics. Thus, OCTA imaging can

K. H. Park, T.-W. Kim (eds.), *OCT Imaging in Glaucoma*,
https://doi.org/10.1007/978-981-16-1178-0_6

not only help evaluate glaucoma patients in the clinic, but enables studies investigating the relationship of parapapillary microvascular compromise to the pathophysiologic features of glaucomatous optic neuropathy.

2 Basic Principles

Vascular imaging by OCTA is based on the OCT volume scan, which is auto-segmented and showed en-face to provide a view of the vasculature in individual segmented layers of the retina and choroid. The basic principle of OCTA is the taking of sequential B-scans at the same retinal location, followed by analysis to determine if there were any changes in the amplitude (intensity signal-based technique) (Jia et al. 2012a) and/or phase (phase signal-based technique) (Wang 2010) of the scan (Kashani et al. 2017). Changes signify movement of the retinal tissue at this location. This movement is thought to be due to the flow of red blood cells (RBCs) in the vasculature (i.e., functioning blood vessels Fig. 1). In contrast to traditional angiography (i.e., fluorescein or indocyanine green angiography), OCTA produces a static map of the vascular network without providing true information regarding blood flow or vascular leakage. Various systems are commercially available, with these systems using different acquisition, saving, and analytic processes (Li et al. 2018; Corvi et al. 2018).

3 Production of an En-Face Image from Segmented Tissue Layers

A two-dimensional (2D) en-face vascular map can be constructed from the 3D volume data obtained from any layer of interest. OCTA systems usually have preset layers of interest, with these layers segmented through an automated process. Although the preset layers vary slightly among systems, most systems provide images segmented in the radial peripapillary capillary plexus (RCP), superficial capillary plexus (SCP), deep capillary plexus (DCP), and choriocapillaris/choroidal layers (Fig. 2) (Spaide et al. 2015a). Manual segmentation can also be performed.

Most OCTA platforms generate en-face OCTA and B-scan OCT images with vascular signal overlay, enabling the in-tandem visualization of both the vasculature and structure (Fig. 2).

4 Strengths of OCTA

The outstanding feature of OCTA is that it does not require injection of a contrast dye, thus eliminating both systemic and local adverse effects. A single volume scan requires only a few seconds. OCTA has a high reproducibility and repeatability (Venugopal et al. 2018). Unlike conventional 2D angiography, OCTA is based on 3D images, allowing the depth-resolved en-face visualization

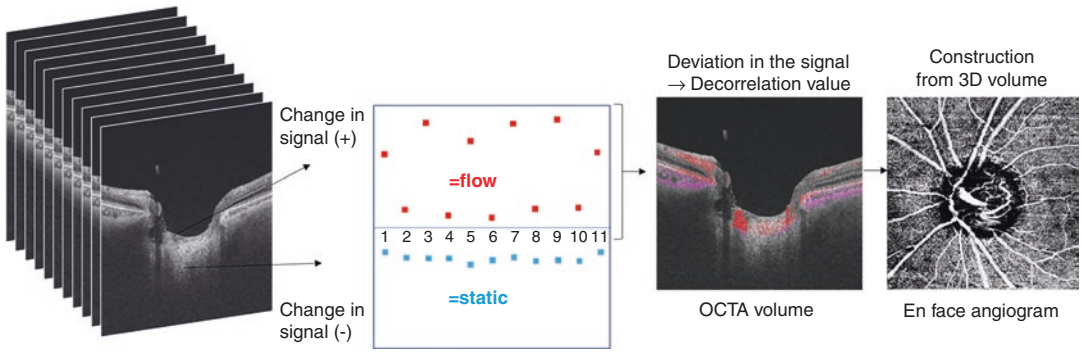

Fig. 1 Basic principle of OCTA. Sequential B-scans are taken at the same location, and compared to detect any changes in signal. A significant change in signal is thought to indicate blood flow. Alterations in signal are assessed mathematically to provide a decorrelation signal representing the amount of blood flow at that location. OCTA, optical coherence tomography angiography

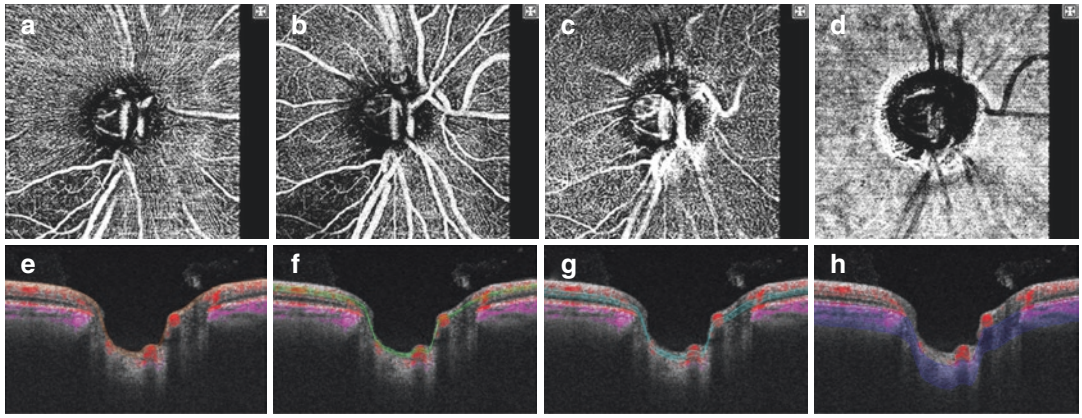

Fig. 2 Peripapillary OCTA images of a glaucomatous eye, obtained in the 4.5 × 4.5 mm area centered on the ONH using DRI OCT Triton (Topcon, Tokyo, Japan). The *upper panel* shows en-face OCTA images segmented in the (**a**) RCP, (**b**) SCP, (**c**) DCP, and (**d**) choroidal layers. The *lower panel* shows B-scan images (**e**–**h**) indicating the layers segmented to produce the en-face images in the *upper panel*. RCP, SCP, and DCP are segmented in the RNFL (**e**), GCL (**f**), and INL (**g**), respectively. OCTA, optical coherence tomography angiography; ONH, optic nerve head; RCP, radial peripapillary capillary plexus; SCP, superficial capillary plexus; DCP, deep capillary plexus; RNFL, retinal nerve fiber layer; GCL, ganglion cell layer; INL, inner nuclear layer

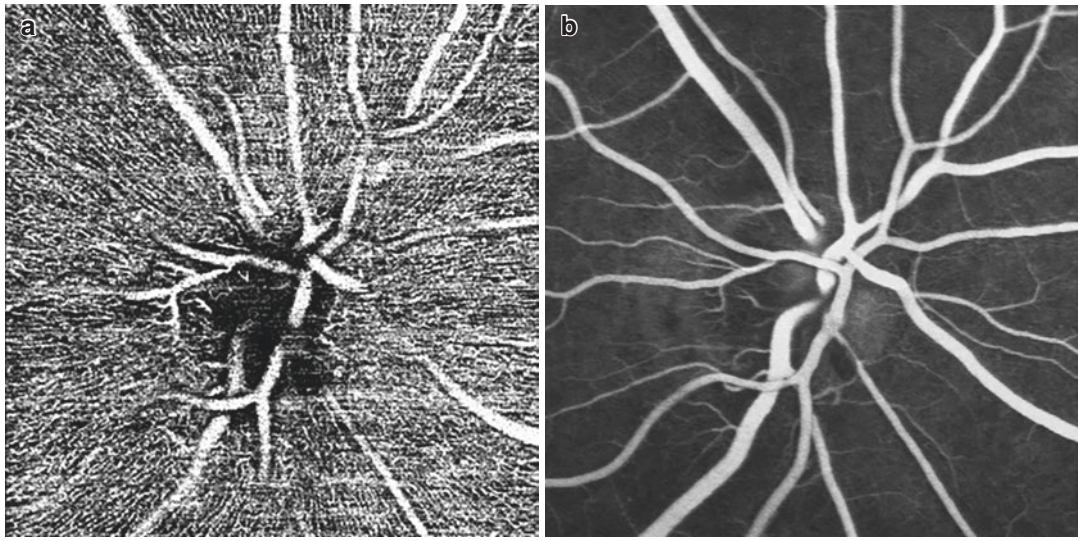

Fig. 3 (**a**) En-face OCTA image of the RCP and (**b**) an FA image of a healthy eye. The RCP is seen in exquisite detail on OCTA (**a**), whereas visualization on FA is poor (**b**). OCTA image was obtained using DRI OCT Triton (Topcon) and FA image was obtained Spectralis HRA + OCT (Heidelberg Engineering, Heidelberg, Germany). OCTA, optical coherence tomography angiography; RCP, radial peripapillary capillary plexus; FA, fluorescein angiography

of the different retinal capillary plexuses that cannot be distinguished by conventional fluorescein angiography (FA, Fig. 3). OCTA has been shown superior to traditional FA in imaging the RCP and DCP (Spaide et al. 2015a).

5 Limitations of OCTA

In contrast to traditional angiography (i.e., fluorescein or indocyanine green angiography), OCTA produces a static map of the vascular net-

work and therefore does not provide true information regarding blood flow or vascular leakage. Quantitative assessment of flow speed using OCTA is currently unreliable.

OCTA is also prone to image artifacts resulting from patient motion, projection from superficial retinal vessels, and segmentation errors (Spaide et al. 2015b; Ghasemi Falavarjani et al. 2017). Because OCTA involves scans of the same area repeated multiple times, motion artifacts are likely to be caused by microsaccades, breathing, and cardiac cycle changes (Fig. 4). Blinking artifacts are caused by eye closure during image capture (Fig. 4). Fluctuating shadows from RBCs in superficial vessels can cast extra flow signals to deeper vascular networks, leading to projection artifacts (Fig. 4). Refracted, reflected, absorbed, or passing of the OCT beam through a vessel can generate false blood flow signals.

Various motion correction and eye-tracking technologies are applied to each OCTA system to reduce motion artifacts (Li et al. 2018). A recently developed projection resolved technique has been incorporated into OCTA (Takusagawa et al. 2017).

6 Evaluation of OCTA in Glaucoma

OCTA has been shown useful in distinguishing between glaucomatous and healthy eyes. As a diagnostic tool, OCTA can serve as an addition to conventional methods, or can substitute for the latter in eyes in which conventional tools are inconclusive, including eyes with high myopia (Shin et al. 2019; Lee et al. 2020a, b; Na et al. 2020) and advanced glaucoma (Kim et al. 2019a; Moghimi et al. 2019). OCTA may also be useful in the detection of glaucoma progression (Lee et al. 2019, c; Park et al. 2019; Hou et al. 2020).

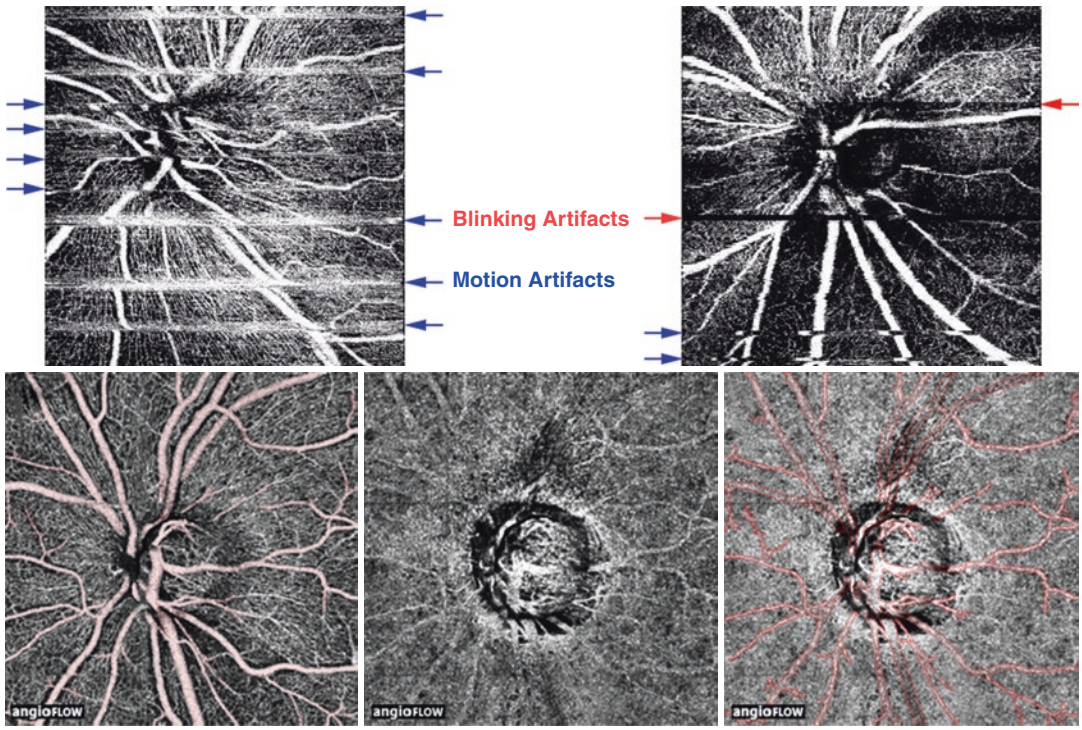

Fig. 4 Artifacts in OCTA. The *upper panel* shows en-face images of the SCP with motion (*blue arrows*) and blinking (*red arrows*) artifacts. The *lower panel* shows an example of a projection artifact. Signals of retinal vessels (colored in *light-red*) in the OCTA image of the SCP layer (**a**) are also observed (vessels demarcated with *red lines*) in the image of the choroidal layer (**b**, **c**). Images were obtained using DRI OCT Triton (Topcon) and RTVue XR Avanti (Optovue, Fremont Inc, California, USA), respectively. OCTA, optical coherence tomography angiography; SCP, superficial capillary plexus

6.1 Macular Imaging

OCTA imaging of the macula usually involves an area ranging from 3 × 3 to 9 × 9 mm^2 centered on the fovea. Vessel density (VD) in the segmented retinal layers and foveal avascular zone (FAZ) are the two most frequently used parameters in glaucoma evaluation.

6.1.1 FAZ

The FAZ is a region lacking capillaries at the center of the macula surrounded by interconnected capillary networks. FAZs are larger in area and have a more irregular shape in eyes with glaucoma than in healthy eyes (Zivkovic et al. 2017; Choi et al. 2017). These findings are topographically correlated with the location of visual field (VF) defects (Fig. 5)

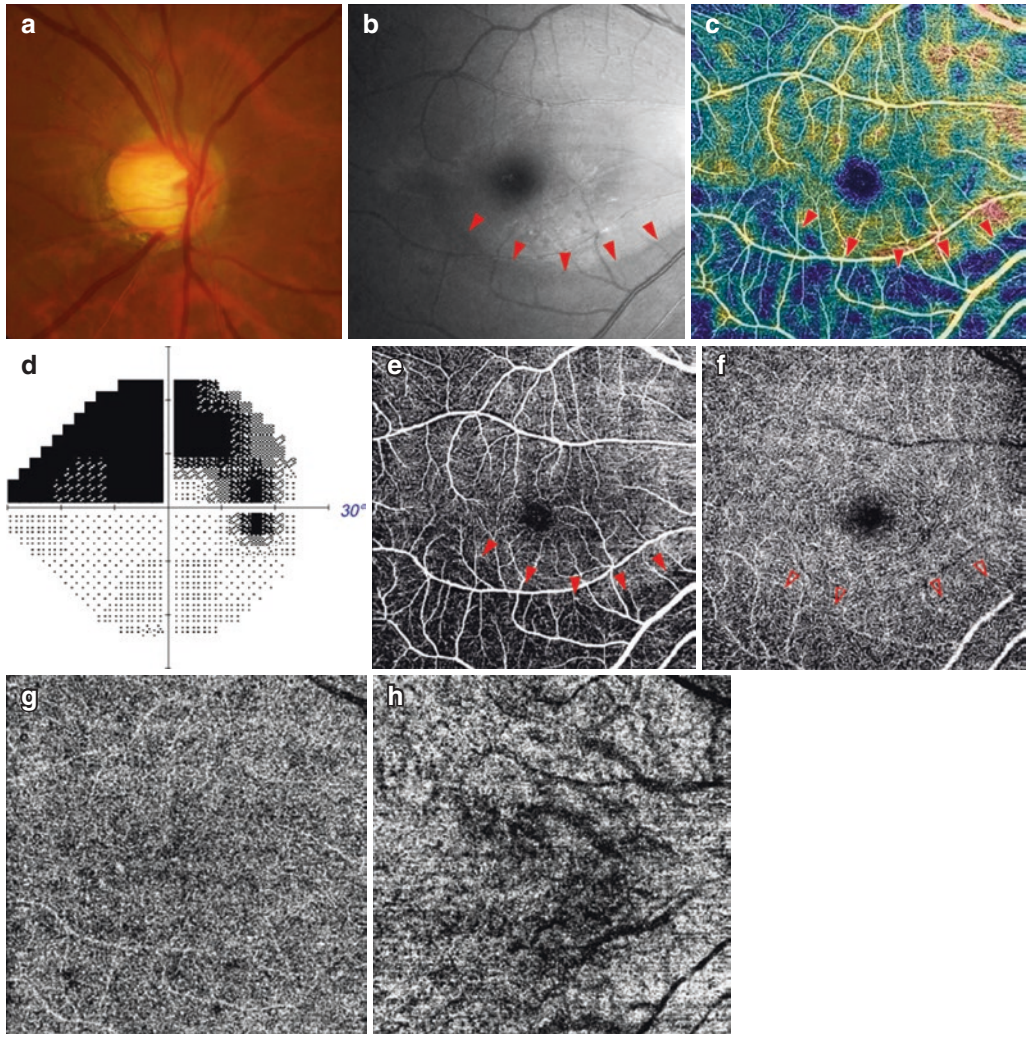

Fig. 5 Findings of macular OCTA (DRI OCT Triton, Topcon) in a glaucomatous eye with inferior ONH damage. The *upper panel* shows a color disc photograph (**a**), a red-free fundus photograph (**b**), an OCTA VD map (**c**), and a gray scale plot of VF examination (**d**). The *blue color* in the VD map (**c**, *arrowheads*) coincides with the localized RNFL defect shown in the red-free photograph (**b**, *arrowheads*). The *lower panel* shows en-face OCTA images of a 6.0 × 6.0 mm^2 area centered on the macula, segmented in the layers of SCP (**e**), DCP (**f**), choriocapillaris (**g**), and choroid (**h**). The localized reduction in macular VD is clearly visualized in the SCP (**e**, *arrowheads*), but less clearly in the DCP (**f**, *arrowheads*), and is not visible in the choriocapillaris (**g**) and choroidal (**h**) layers. Note that choroidal vessels are not clearly visible in the choroidal OCTA image (**h**), because of signal attenuation by the pigmented RPE and choriocapillaris. OCTA, optical coherence tomography angiography; ONH, optic nerve head; VD, vessel density; VF, visual field; RNFL, retinal nerve fiber layer; SCP, superficial capillary plexus; DCP, deep capillary plexus; RPE, retinal pigment epithelium

(Kwon et al. 2017a). FAZs are larger in eyes with pseudoexfoliative glaucoma than with open angle glaucoma (Philip et al. 2019). Moreover, FAZs are larger in women than in men, especially in older women (Gomez-Ulla et al. 2019), indicating that age and gender should be considered when assessing FAZs.

6.1.2 Macular Microvessel Density

Reduced macular VD has been observed in both the SCP and DCP of glaucomatous eyes (Choi et al. 2017; Wu et al. 2019; Kim et al. 2020a; Lommatzsch et al. 2018; Akil et al. 2017). These changes in macular microvessels were found to be well correlated with the degrees of structural (Wu et al. 2019; Kim et al. 2020a; Lommatzsch et al. 2018; Akil et al. 2017; Hou et al. 2019; Chung et al. 2017; Rao et al. 2017a; Lu et al. 2020) and functional (Lommatzsch et al. 2018; Lu et al. 2020) damage (Fig. 5) and were independent of age-related capillary loss (Wu et al. 2019). Choroidal imaging is limited in the macular area because the light is scattered or attenuated by the pigmented RPE and choriocapillaris with dense vascular structure (Fig. 5).

6.2 Peripapillary Imaging

Scanning of the ONH and peripapillary area is the most widely used OCTA imaging in glaucoma evaluation. Evaluation of the peripapillary microvasculature using OCTA helps to diagnose glaucoma (Moghimi et al. 2019; Liu et al. 2015; Enders et al. 2020; Rolle et al. 2019; Akagi et al. 2016; Yarmohammadi et al. 2018) and predict its progression (Jia et al. 2014; Cennamo et al. 2017). Abnormalities in the retinal and/or choroidal microvasculature may indicate reduced ocular perfusion, indicating that OCTA evaluation of the peripapillary microvasculature could shed a light on the vascular theory of glaucoma. However, it remains unclear whether the abnormal microvasculature in glaucomatous eyes is a causal factor in glaucoma pathogenesis or a secondary result of glaucomatous nerve fiber loss.

Peripapillary OCTA images are usually obtained from 3 × 3, 4.5 × 4.5 or 6 × 6 mm^2 areas centered on the ONH. The most common are those from peripapillary 4.5 × 4.5 mm^2 scans (Fig. 1), which have been shown to better detect glaucomatous changes than images from 6.0 × 6.0 mm^2 scans (Chang et al. 2019). However, one study reported that wider scans were superior in investigating capillary loss during early stages of glaucoma (Jia et al. 2017).

6.2.1 Optic Nerve Head

OCTA has been shown to detect abnormalities of ONH perfusion in glaucoma (Chung et al. 2017; Jia et al. 2012b, 2014). Imaging of the deeper ONH tissues (i.e., the lamina cribrosa [LC]) is limited by the shadowing or projection of large retinal vessels. However, there are studies where deep ONH tissues, including the LC and prelaminar tissues, have been imaged successfully (Numa et al. 2018; Kim et al. 2018, 2019b). The microvasculature in the LC was found to be negatively associated with the LC curvature, an indicator of mechanical stress derived from translaminar pressure difference (Fig. 6) (Kim et al. 2019b). In addition, reversal of the LC curvature following surgical IOP reduction was positively associated with the increased microvascular density in the LC (Fig. 6) (Kim et al. 2018). These findings indicate that LC deformation caused by mechanical stress can also influence perfusion of the ONH axons by compressing the laminar capillaries (Burgoyne et al. 2005).

6.2.2 Peripapillary Retina

Peripapillary retinal microvasculature can be assessed in the RCP, SCP, and DCP. In glaucoma, reduced VD is more prominent in the superficial than in the deeper layers (Liu et al. 2019). VD has been shown to correlate with both structural (Chung et al. 2017; Rao et al. 2017a; Enders et al. 2020; Lee et al. 2016a; Ichiyama et al. 2017) and functional (Liu et al. 2015; Akagi et al. 2016; Ichiyama et al. 2017; Shin et al. 2017a) damage, and is an excellent parameter for diagnosing glaucoma (Liu et al. 2015; Rolle et al. 2019; Bekkers et al. 2020). In patients with localized RNFL defects, reduced VD in the superficial retina was observed to coincide with wedge shaped RNFL defects (Fig. 7), suggesting that the

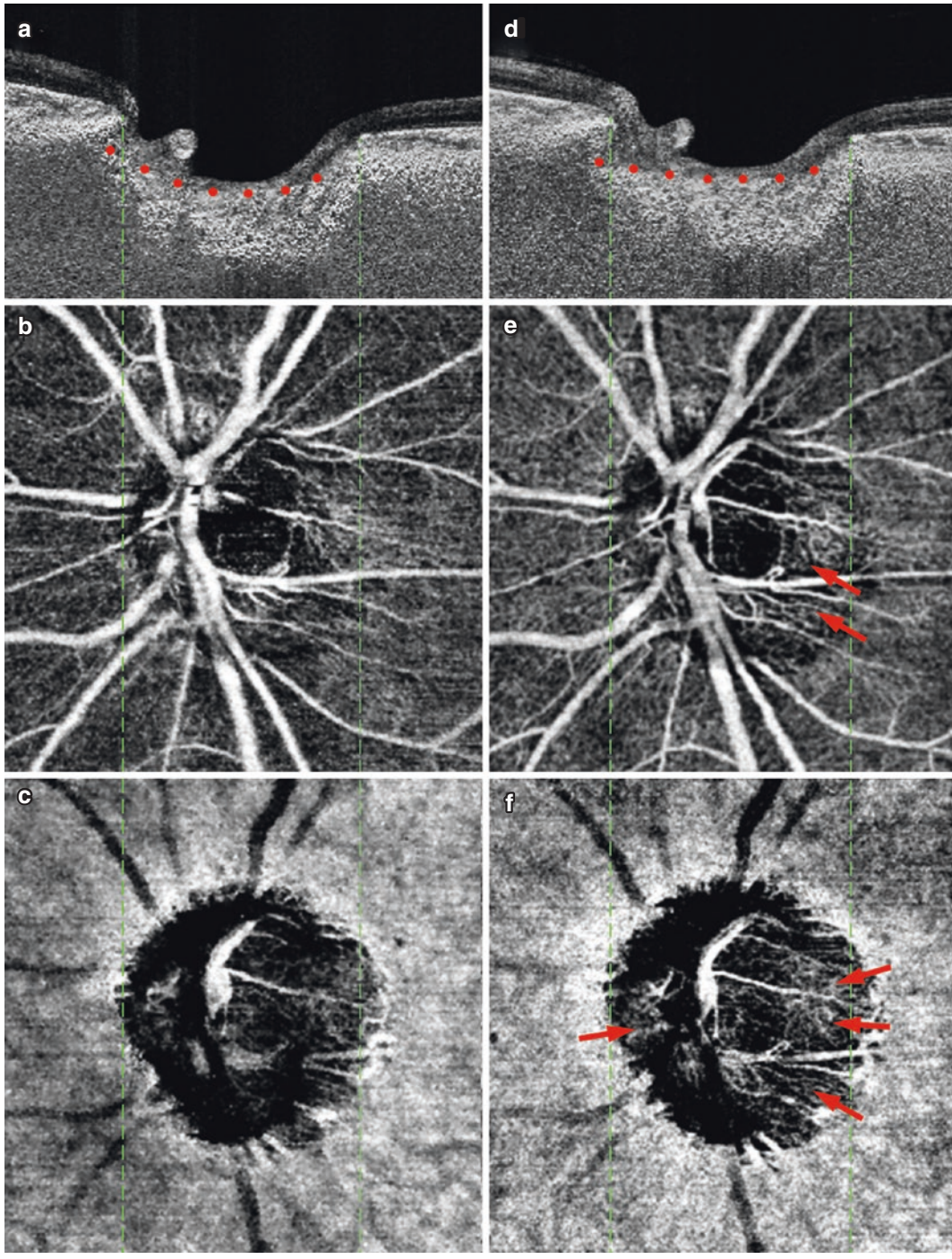

Fig. 6 A glaucomatous eye that underwent trabeculectomy, showing that reduction of the LC curvature (*red glyphs*) was associated with an increased microvascular density in ONH tissues (*arrows*). Images in the left column were obtained 1 day preoperatively (**a**–**c**), and images in the right column were obtained 3 months postoperatively (**d**–**f**). The top row (**a**, **d**) shows B-scan images of the central ONH, illustrating that the LC curvature was reduced after surgery (*red glyphs*). Note the increased microvasculature (*arrows*) in the prelaminar tissue (**e**) and in the LC (**f**). Images were obtained using DRI OCT Triton (Topcon). LC, lamina cribrosa; ONH, optic nerve head

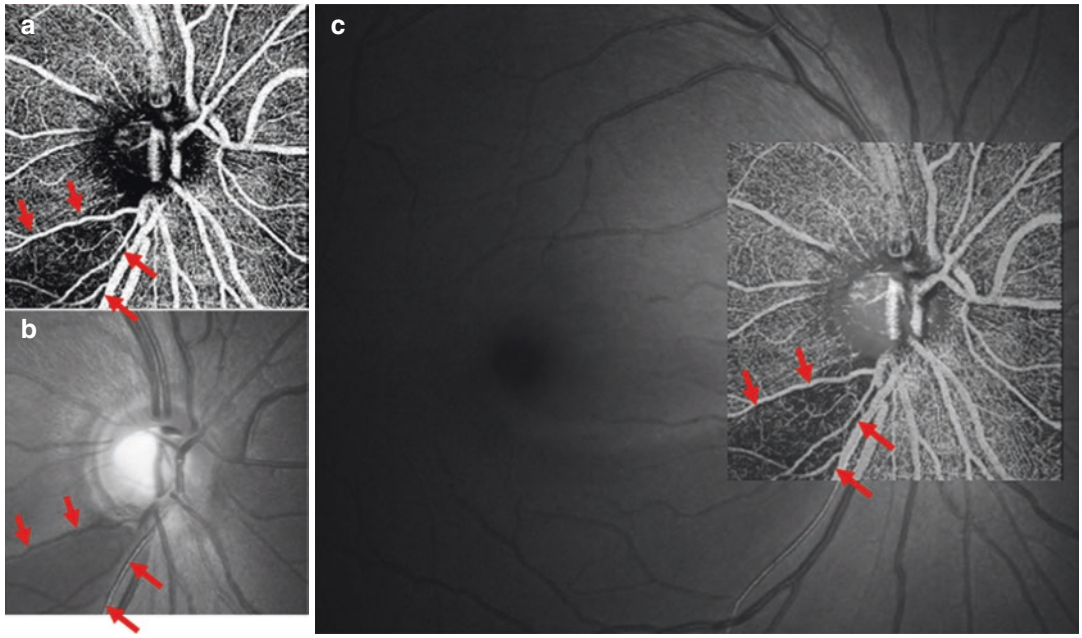

Fig. 7 En-face OCTA image of the superficial retina, including the RCP and SCP (**a**); a red-free fundus photograph (**b**); and the red-free fundus photograph superimposed on the en-face angiogram (**c**). The vascular impairment shown by OCTA appears to be identical to the RNFL defects evident in red-free photographs (*arrows*). OCTA Images were obtained using DRI OCT Triton (Topcon). OCTA, optical coherence tomography angiography; RCP, radial peripapillary capillary plexus; SCP, superficial capillary plexus; RNFL, retinal nerve fiber layer

decrease in retinal microvasculature is likely a secondary loss or closure of capillaries in areas of glaucomatous RNFL atrophy (Lee et al. 2016a).

6.2.3 Peripapillary Choroid

The peripapillary area, which is distinct from the macular area, frequently accompanies an area with atrophic RPE, thus allowing detailed OCTA imaging of the parapapillary choroidal microvasculature. Focal dropout of the juxtapapillary choroidal microvasculature has been observed in glaucomatous eyes (Suh et al. 2016), which had a good topographic correlation with glaucomatous RNFL (Lee et al. 2017a) and VF (Akagi et al. 2016; Suh et al. 2018) defects. Microvasculature dropout (MvD) in the peripapillary choroid has been shown to coincide with perfusion defects detected by indocyanine green angiography (ICGA, Fig. 8) (Lee et al. 2017b), indicating that MvD is likely indicative of a true perfusion defect in the choroid. Glaucoma progression was found to be faster in eyes with than without juxtapapillary choroidal MvD (Lee et al. 2019, 2020c).

6.3 Anterior Segment Imaging

Anterior segment OCTA has been utilized to image the vasculature in the conjunctiva and intrasclera. Hyperemia of the anterior segment, which has been associated with elevated IOP, as well as post-trabeculectomy avascular bleb could be imaged using the anterior segment OCTA (Akagi et al. 2019a, b). The clinical usefulness of anterior segment OCTA imaging in glaucoma remains to be determined. Experimental studies have attempted to image the aqueous humor outflow tract (Zhang et al. 2020; Gottschalk et al. 2019).

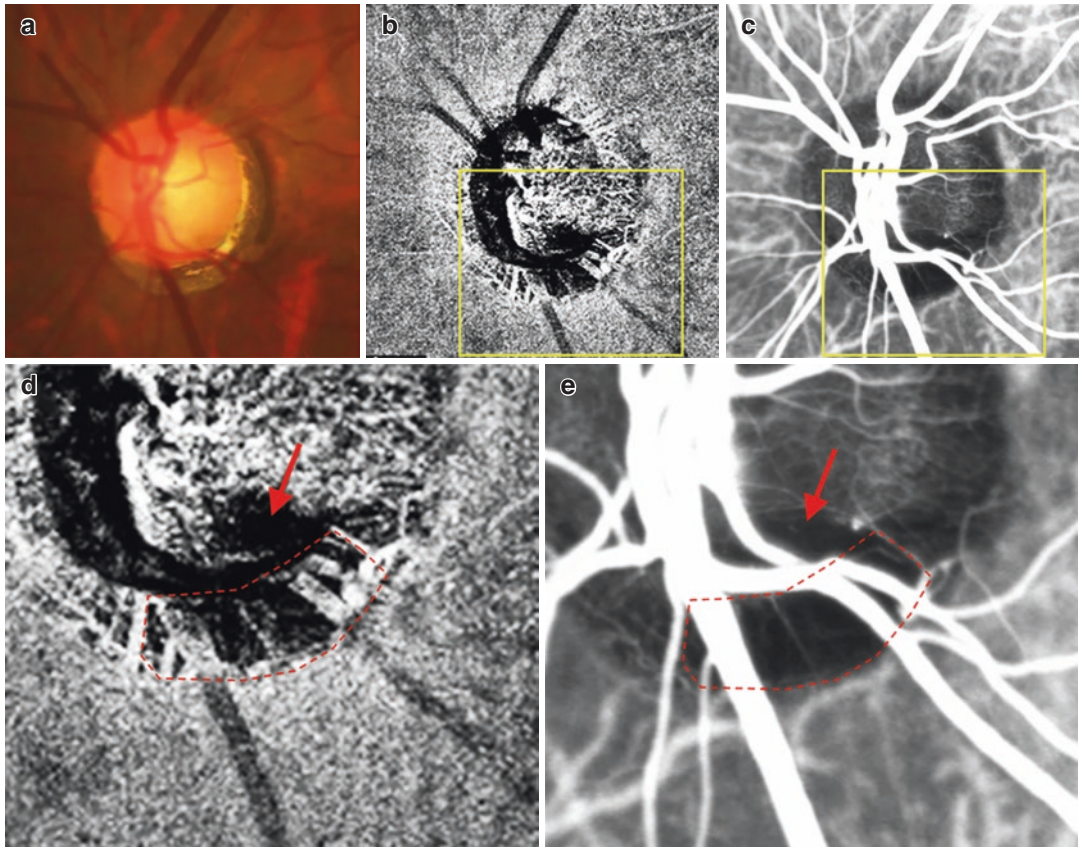

Fig. 8 Color disc photograph (**a**), en-face OCTA image of the choroid (**b**), and ICGA image at the peak phase (36 s, **c**) in a glaucomatous eye with an MvD. Images (**d**) and (**e**) are magnified images of (**b**) and (**c**), respectively. The parapapillary capillary dropout shown in the OCTA image exactly coincides with the perfusion defect shown in the ICGA image (areas demarcated by *dashed lines*). Focal dropout of intrapapillary microvessels is also observed in both the OCTA and ICGA images (*arrows*). OCTA and ICGA images were obtained using DRI OCT Triton (Topcon) and Spectralis HRA + OCT (Heidelberg Engineering), respectively. MvD, microvasculature dropout; OCTA, optical coherence tomography angiography; ICGA, indocyanine green angiography

7 Clinical Use of OCTA in Glaucoma Patients and OCTA in Glaucoma Research

7.1 Diagnosis of Glaucoma

Variable OCTA parameters can be useful in diagnosing glaucoma, with their diagnostic power being comparable to those of OCT (Yarmohammadi et al. 2018; Cennamo et al. 2017; Kumar et al. 2016) or VF examination (Kumar et al. 2016; Yarmohammadi et al. 2016). Sectors of the SCP and DCP with reduced microvessel density (Akagi et al. 2016; Lee et al. 2016a; Shin et al. 2017a) and the locations of MvD (Akagi et al. 2016; Lee et al. 2017a) and abnormal FAZ (Kwon et al. 2017a) were all well correlated with the locations of glaucomatous RNFL and VF loss. The magnitude of VD reduction (Cennamo et al. 2017; Shin et al. 2017a; Yarmohammadi et al. 2016) and MvD size (Lee et al. 2017a; Shin et al. 2018) and FAZ (Kwon et al. 2017a, b) also showed good correlations with the severity of glaucomatous damage.

The advantage of using OCTA in glaucoma assessment is that it is unaffected by the low reflectance of the RNFL or structural deformations of the optic nerve, such as optic disc tilt or PPA. Therefore, OCTA can be useful for evaluating glaucomatous damage in highly myopic eyes (Fig. 9) (Na et al. 2020).

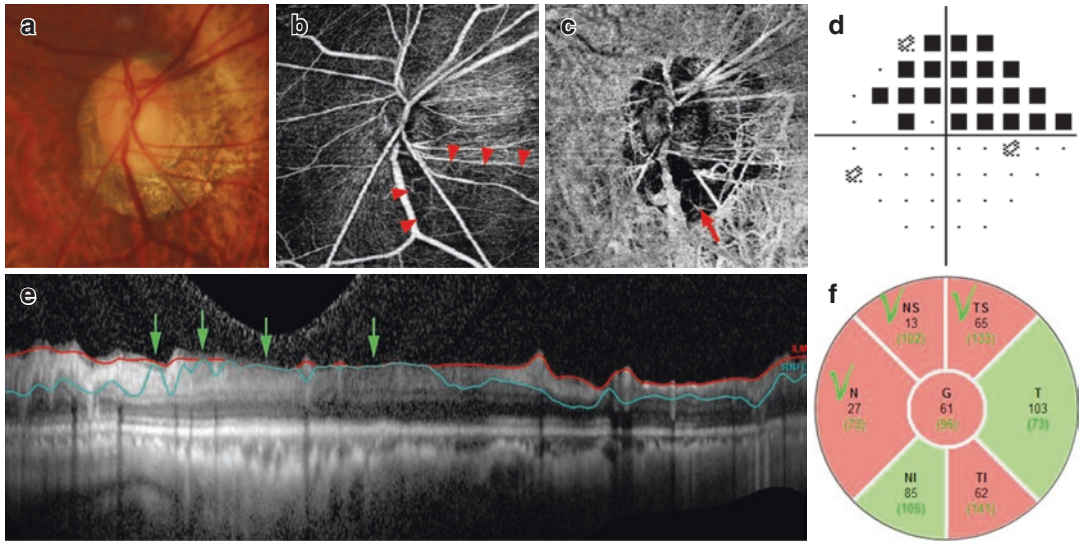

Fig. 9 A highly myopic glaucomatous eye with inferior ONH damage. Color disc photograph (**a**) shows inferior neuroretinal rim loss. En-face OCTA images (**b**, **c**) clearly show reduced retinal vessel density (*arrowheads*) and a choroidal MvD (*red arrow*) in the inferior hemisphere. The location of capillary loss corresponded well with the location of hemifield VF defect (**d**). In contrast, an OCT peripapillary scan (**e**) failed to demonstrate RNFL loss accurately, a failure that was due to segmentation error. The *light-green arrows* indicate the locations of segmentation errors resulting in false positive color codes in the N, NS, and TS sectors (**f**). OCTA images were obtained using DRI OCT Triton (Topcon). G, global; TS, temporal superior; T, temporal; TI, temporal inferior; NI, nasal inferior; N, nasal; NS, nasal superior; OCTA, optical coherence tomography angiography; MvD, microvasculature dropout; VF, visual field; OCT, optical coherence tomography; RNFL, retinal nerve fiber layer

In addition, OCTA measurements of microvessel density are less affected by the thickness of large vessels and are therefore unaffected by a floor effect. These advantages make OCTA particularly useful in evaluating glaucomatous damage in eyes with advanced damage (Kim et al. 2019a; Moghimi et al. 2019). OCTA can also be useful for monitoring disease progression in eyes with advanced glaucoma, with the rate of macular VD loss being more rapid than the rate of structural thinning (Hou et al. 2020).

The clinical usefulness of OCTA in patient diagnosis requires a technique to enhance image quality, a reliable algorithm to accurately quantify microvessel damage, and normative data based on a diverse population.

7.2 Study of Vascular Theory

The increased clinical availability of OCTA has led to an increase in the number of studies assessing the link between the OCTA vasculature and decreased ocular perfusion in the pathogenesis of glaucoma. Reductions in retinal microvasculature have been shown to precede VF damage in early preperimetric glaucoma (Lu et al. 2020; Kumar et al. 2016), with reduced retinal VD being more pronounced in glaucomatous eyes with lower than higher IOP (Xu et al. 2018). Lower baseline VD in the retina has been associated with a faster rate of RNFL thinning, suggesting that reduced ocular perfusion may have led to faster glaucomatous damage (Moghimi et al. 2018). Decreased VD on OCTA may represent dysfunctional retinal ganglion cells with lower metabolic demands. However, the findings of various studies have been inconsistent (Hou et al. 2019; Hirasawa et al. 2021; Kim et al. 2017; Mursch-Edlmayr et al. 2020; Bojikian et al. 2016), with results to date unable to determine whether reductions in retinal microvasculature are indicative of reduced ocular perfusion causing ischemic axonal damage. Based on our study, showing an exact overlap between localized RNFL defects and reduced retinal microvasculature (Lee et al. 2016a), this is more likely to be a secondary phenomenon

resulting from glaucomatous atrophy of the RNFL and GCL (Fig. 7).

The retinal microvasculature consists of capillaries supplied by the central retinal artery system. However, the ONH is supplied with blood by the short posterior ciliary artery (SPCA). Layer segmentation in OCTA allows individual examination of the microvasculature supplied by the SPCA. The peripapillary choroidal microvasculature is of particular interest in understanding vascular theory, because this microvasculature is supplied by the SPCA, which also perfuses deep ONH tissues. OCTA has identified localized MvD in the peripapillary choroid of patients with glaucoma (Akagi et al. 2016). This localized MvD has been associated with both the location (Ichiyama et al. 2017; Lee et al. 2017a) and severity (Ichiyama et al. 2017; Suh et al. 2016) of glaucomatous damage. Areas of MvD were found to correspond to areas of perfusion defects on ICGA, indicating that MvD represents a true vascular compromise (Fig. 8) (Lee et al. 2017b). The presence of MvD was found to be associated with lower systemic blood pressure and lower ocular perfusion pressure (Suh et al. 2016; Lee et al. 2017b, 2018). In addition, MvD was a strong predictor of early parafoveal scotoma (Lee et al. 2018; Kwon et al. 2018), which is thought to represent systemic vascular risk factors (Park et al. 2011; Yoo et al. 2017). Taken together, these findings suggest that MvD may be a key to understanding vascular pathogenesis. MvD has been shown to be a strong predictor of glaucoma progression (Lee et al. 2019, 2020c; Kwon et al. 2019). A prospective study found that the occurrence of MvD was the second strongest predictor of glaucoma progression, with larger LC curvature, an indicator of mechanical stress, being the strongest predictor (Fig. 10) (Lee et al. 2019). Therefore, areas of MvD may represent the location of ischemia affecting the viability of axons and retinal ganglion cells, causing ischemic insult in addition to mechanical stress. Interestingly, areas of MvD could be identified in nonglaucomatous healthy eyes of patients with low systemic blood pressure profiles (Kim et al. 2020b). Further

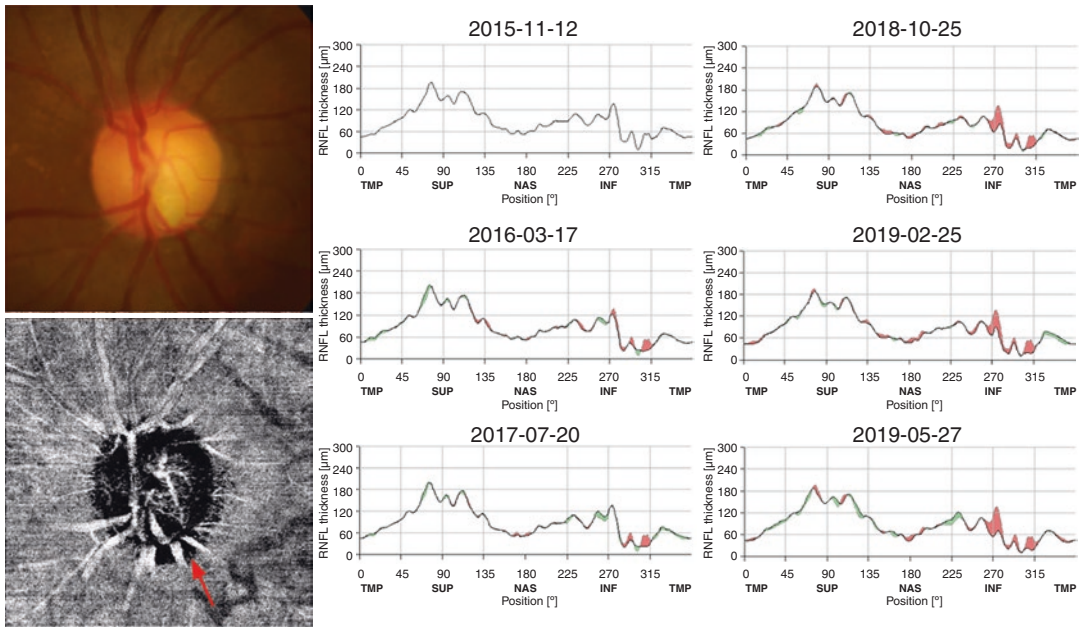

Fig. 10 Rapidly progressing glaucoma in an eye with an MvD in the inferior sector (*arrow*). The *right panel* shows progressive changes in RNFL thickness and rapid progressive thinning of the RNFL in the inferior sector (*red-colored area*). The diurnal IOP ranged from 15 to 17 mmHg before treatment and was maintained within a range of 10–12 mmHg during the entire treatment period. The OCTA image was obtained using DRI OCT Triton (Topcon). TMP, temporal; SUP, superior; NAS, nasal; INF, inferior; MvD, microvasculature dropout; RNFL, retinal nerve fiber layer; IOP, intraocular pressure

studies are warranted to determine whether such eyes would eventually undergo structural damage.

MvD has been frequently found in glaucomatous eyes with PPA β- and γ-zones associated with myopia. However, the β- and γ-zones have different pathomechanisms (Dai et al. 2013; Kim et al. 2013), and MvDs observed in these zones differ in their underlying microstructures, suggesting differences in the pathogenesis of parapapillary MvD in the β- and γ-zones (Fig. 11) (Lee et al. 2017c, d).

MvD-like structures have also been identified in nonglaucomatous eyes, including in highly myopic eyes without glaucoma (Fig. 12) (Kim et al. 2020c) and in eyes with compressive optic neuropathy (Fig. 13) (Lee et al. 2020d). However,

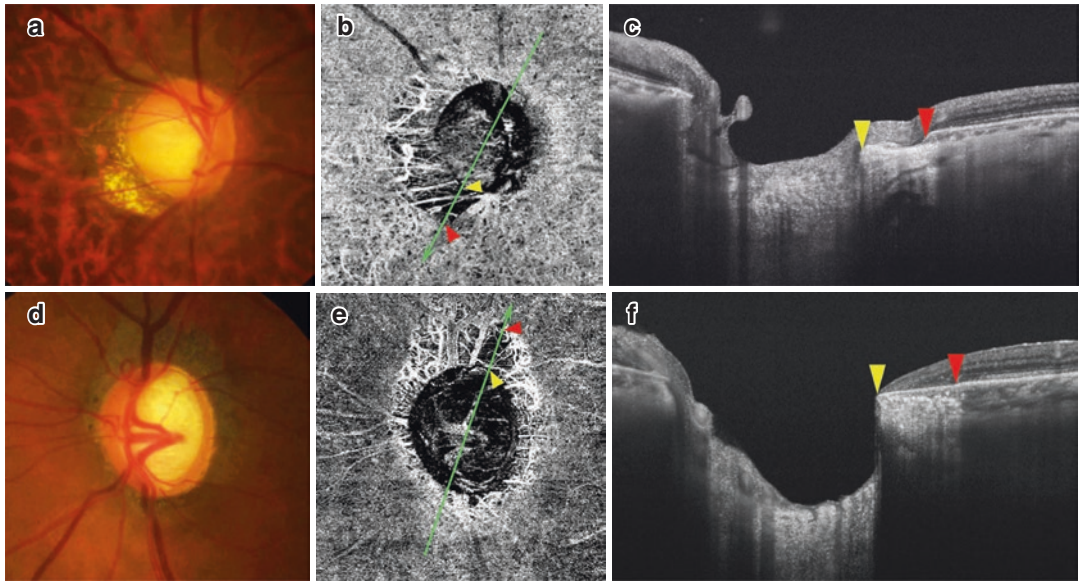

Fig. 11 Glaucomatous eyes having MvD in the γ-zone (*upper*) and β-zone (*lower*). Color disc photographs show PPA consisted of γ-zone (**a**) and β-zone (**d**) in each eye. *Light-green arrows* (**b**, **e**) indicate the locations of the B-scans in (**c**) and (**f**), respectively. *Yellow* and *red arrowheads* (**b**, **c**, **e**, **f**) indicate the points of the clinical disc margins (proximal MvD margins) and the distal margins of the MvD, respectively. Although choroidal tissue of noticeable thickness is present under the MvD in the β-zone (**f**), only the border tissue of Elschnig, which does not contain choroidal tissue, is present under the MvD in the γ-zone (**c**), suggesting differences in the pathogenesis of parapapillary MvD in the β- and γ-zones. OCTA images were obtained using DRI OCT Triton (Topcon). MvD, microvasculature dropout; PPA, parapapillary atrophy; OCTA, optical coherence tomography angiography

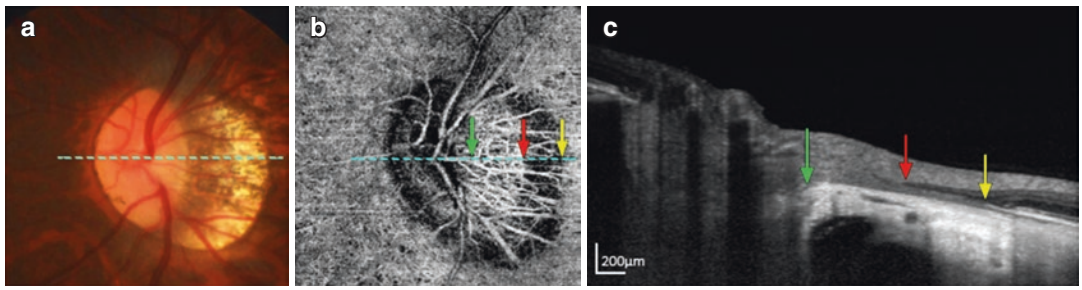

Fig. 12 A nonglaucomatous eye with high myopia. En-face choroidal OCTA image (**b**), showing an MvD-like structure in the non-juxtapapillary area (between the *red* and *yellow arrows*). The *light-green arrow* indicates the clinical optic disc margin. B-scan image (**c**), showing that the MvD-like structure did not consist of choroid, but mainly of border tissue and scleral flange. *Dashed lines* (**a**, **b**) indicate the location from which the B-scan image in (**c**) was obtained. OCTA image was obtained using DRI OCT Triton (Topcon). OCTA, optical coherence tomography angiography; MvD, microvasculature dropout

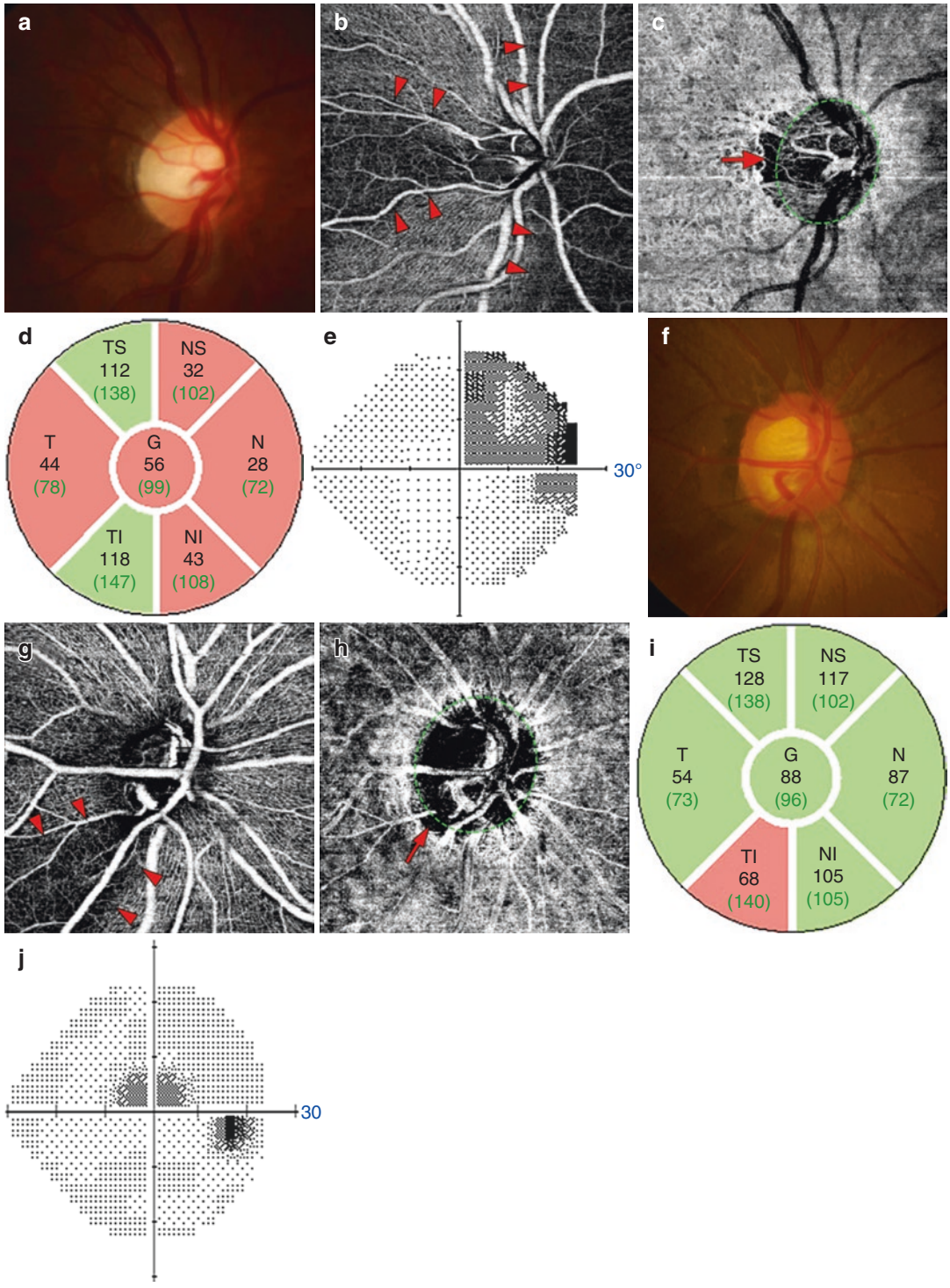

Fig. 13 Findings in a patient with compressive optic neuropathy associated with a pituitary adenoma (*upper panel*) and a patient with glaucomatous optic neuropathy (*lower panel*). The patterns and locations of reduced retinal VD (*arrowheads*) and choroidal capillary dropouts (*arrows*) in the en-face OCTA images clearly differed in these two eyes. OCTA images were obtained using DRI OCT Triton (Topcon). VD, vessel density; OCTA, optical coherence tomography angiography

the locations, structures, and accompanying clinical characteristics of these MvDs differed from the MvDs identified in glaucoma, suggesting that their pathogeneses and pathogenic meanings may differ from those of MvDs observed in glaucomatous eyes. These differences, however, remain to be determined.

7.3 Evaluation of Perfusion Recovery After Treatment

Reduced mechanical stress is thought to increase microvasculature in the peripapillary retina and in ONH tissues. IOP reduction following filtering surgery has been found to induce reversal of the deformed LC (Lee et al. 2012, 2016b). Studies using OCTA have shown that the increase in microvasculature was associated with the magnitude of LC reversal after IOP lowering surgery (Fig. 6) (Kim et al. 2018; Shin et al. 2017b), suggesting that this reversal of LC relieves compression on the capillaries within the LC trabeculae, potentially increasing blood flow to the ONH axons.

Microvasculature changes after application of topical medications have not yet been clarified. Topical application of the Rho-assisted coiled-coil forming protein kinase inhibitor ripasudil was found to enhance peripapillary VD, whereas topical application of the alpha-2 agonist brimonidine did not (Chihara et al. 2018). Because both medications reduce IOP to a similar extent, the increase in VD induced by ripasudil may not be caused by its reduction of mechanical stress but by its vasodilatory effect.

7.4 Differences Among Types of Glaucoma

OCTA does not seem to differentiate among different types of glaucoma. Studies have compared OCTA findings in eyes with normal-tension and high-tension glaucoma (Xu et al. 2018; Mursch-Edlmayr et al. 2020; Bojikian et al. 2016) and in eyes with primary angle-closure, primary open angle, and pseudoexfoliative glaucoma (Rao et al. 2017b; Jo et al. 2020; Simsek et al. 2020), but most of these studies failed to detect significant differences.

8 Conclusions

OCTA can provide reproducible information about the microvasculature in the ONH and retina, with an ability to diagnose glaucoma comparable to that of OCT and VF examinations. OCTA may therefore be a useful addition to these latter methods in diagnosing glaucoma, particularly when the findings from these conventional methods are inconclusive. The rapid, noninvasive, and reproducible nature of OCTA examinations may facilitate the evaluation of glaucoma patients in busy clinics.

En-face OCTA images show the microvascular structure in individual retinal layers and ONH tissues. These findings correspond to those of conventional angiography, and can even visualize vascular layers not evaluable by conventional methods. This capacity enables OCTA to assess individual microvasculature systems supplying the ONH and peripapillary area, resulting in increased understanding of vascular pathogenesis in glaucoma.

Current OCTA systems are limited by artifacts that affect image quality, by an inability to quantify blood flow, and by the lack of a reliable normative database. However, technologies are rapidly evolving, and it will not be long before these limitations are overcome.

References

Akagi T, Iida Y, Nakanishi H, et al. Microvascular density in glaucomatous eyes with hemifield visual field defects: an optical coherence tomography angiography study. Am J Ophthalmol. 2016;168:237–49.

Akagi T, Uji A, Okamoto Y, et al. Anterior segment optical coherence tomography angiography imaging of conjunctiva and intrasclera in treated primary open-angle glaucoma. Am J Ophthalmol. 2019a;208:313–22.

Akagi T, Okamoto Y, Tsujikawa A. Anterior segment OCT angiography images of avascular bleb after trabeculectomy. Ophthalmol Glaucoma. 2019b;2(2):102.

Akil H, Chopra V, Al-Sheikh M, et al. Swept-source OCT angiography imaging of the macular capillary net-

work in glaucoma. Br J Ophthalmol. 2017. https://doi.org/10.1136/bjophthalmol-2016-309816.

Bekkers A, Borren N, Ederveen V, et al. Microvascular damage assessed by optical coherence tomography angiography for glaucoma diagnosis: a systematic review of the most discriminative regions. Acta Ophthalmol. 2020;98(6):537–58.

Bojikian KD, Chen CL, Wen JC, et al. Optic disc perfusion in primary open angle and normal tension glaucoma eyes using optical coherence tomography-based microangiography. PLoS One. 2016;11(5):e0154691.

Bonomi L, Marchini G, Marraffa M, Bernardi P, Morbio R, Varotto A. Vascular risk factors for primary open angle glaucoma: the Egna-Neumarkt Study. Ophthalmology. 2000;107(7):1287–93.

Burgoyne CF, Downs JC, Bellezza AJ, Suh JK, Hart RT. The optic nerve head as a biomechanical structure: a new paradigm for understanding the role of IOP-related stress and strain in the pathophysiology of glaucomatous optic nerve head damage. Prog Retin Eye Res. 2005;24(1):39–73.

Cennamo G, Montorio D, Velotti N, Sparnelli F, Reibaldi M, Cennamo G. Optical coherence tomography angiography in pre-perimetric open-angle glaucoma. Graefes Arch Clin Exp Ophthalmol. 2017;255(9):1787–93.

Chang R, Chu Z, Burkemper B, et al. Effect of scan size on glaucoma diagnostic performance using OCT angiography en face images of the radial peripapillary capillaries. J Glaucoma. 2019;28(5):465–72.

Charlson ME, de Moraes CG, Link A, et al. Nocturnal systemic hypotension increases the risk of glaucoma progression. Ophthalmology. 2014;121(10):2004–12.

Chihara E, Dimitrova G, Chihara T. Increase in the OCT angiographic peripapillary vessel density by ROCK inhibitor ripasudil instillation: a comparison with brimonidine. Graefes Arch Clin Exp Ophthalmol. 2018;256(7):1257–64.

Choi J, Kwon J, Shin JW, Lee J, Lee S, Kook MS. Quantitative optical coherence tomography angiography of macular vascular structure and foveal avascular zone in glaucoma. PLoS One. 2017;12(9):e0184948.

Chung JK, Hwang YH, Wi JM, Kim M, Jung JJ. Glaucoma diagnostic ability of the optical coherence tomography angiography vessel density parameters. Curr Eye Res. 2017;42(11):1458–67.

Corvi F, Pellegrini M, Erba S, Cozzi M, Staurenghi G, Giani A. Reproducibility of vessel density, fractal dimension, and foveal avascular zone using 7 different optical coherence tomography angiography devices. Am J Ophthalmol. 2018;186:25–31.

Dai Y, Jonas JB, Huang H, Wang M, Sun X. Microstructure of parapapillary atrophy: beta zone and gamma zone. Invest Ophthalmol Vis Sci. 2013;54(3):2013–8.

Enders P, Longo V, Adler W, et al. Analysis of peripapillary vessel density and Bruch's membrane opening-based neuroretinal rim parameters in glaucoma using OCT and OCT-angiography. Eye (Lond). 2020;34(6):1086–93.

Findl O, Rainer G, Dallinger S, et al. Assessment of optic disk blood flow in patients with open-angle glaucoma. Am J Ophthalmol. 2000;130(5):589–96.

Funaki S, Shirakashi M, Abe H. Parapapillary chorioretinal atrophy and parapapillary avascular area in glaucoma. Nippon Ganka Gakkai Zasshi. 1997;101(7):598–604.

Ghasemi Falavarjani K, Al-Sheikh M, Akil H, Sadda SR. Image artefacts in swept-source optical coherence tomography angiography. Br J Ophthalmol. 2017;101(5):564–8.

Gomez-Ulla F, Cutrin P, Santos P, et al. Age and gender influence on foveal avascular zone in healthy eyes. Exp Eye Res. 2019;189:107856.

Gottschalk HM, Wecker T, Khattab MH, et al. Lipid emulsion-based OCT angiography for ex vivo imaging of the aqueous outflow tract. Invest Ophthalmol Vis Sci. 2019;60(1):397–406.

Graham SL, Drance SM. Nocturnal hypotension: role in glaucoma progression. Surv Ophthalmol. 1999;43(Suppl 1):S10–6.

Hirasawa K, Smith CA, West ME, et al. Discrepancy in loss of macular perfusion density and ganglion cell layer thickness in early glaucoma. Am J Ophthalmol. 2021;221:39–47.

Hitchings RA, Spaeth GL. Fluorescein angiography in chronic simple and low-tension glaucoma. Br J Ophthalmol. 1977;61(2):126–32.

Hou H, Moghimi S, Zangwill LM, et al. Macula vessel density and thickness in early primary open-angle glaucoma. Am J Ophthalmol. 2019;199:120–32.

Hou H, Moghimi S, Proudfoot JA, et al. Ganglion cell complex thickness and macular vessel density loss in primary open-angle glaucoma. Ophthalmology. 2020;127(8):1043–52.

Huber K, Plange N, Remky A, Arend O. Comparison of colour Doppler imaging and retinal scanning laser fluorescein angiography in healthy volunteers and normal pressure glaucoma patients. Acta Ophthalmol Scand. 2004;82(4):426–31.

Ichiyama Y, Minamikawa T, Niwa Y, Ohji M. Capillary dropout at the retinal nerve fiber layer defect in glaucoma: an optical coherence tomography angiography study. J Glaucoma. 2017;26(4):e142–e5.

Jia Y, Tan O, Tokayer J, et al. Split-spectrum amplitude-decorrelation angiography with optical coherence tomography. Opt Express. 2012a;20(4):4710–25.

Jia Y, Morrison JC, Tokayer J, et al. Quantitative OCT angiography of optic nerve head blood flow. Biomed Opt Express. 2012b;3(12):3127–37.

Jia Y, Wei E, Wang X, et al. Optical coherence tomography angiography of optic disc perfusion in glaucoma. Ophthalmology. 2014;121(7):1322–32.

Jia Y, Simonett JM, Wang J, et al. Wide-field OCT angiography investigation of the relationship between radial peripapillary capillary plexus density and nerve fiber layer thickness. Invest Ophthalmol Vis Sci. 2017;58(12):5188–94.

Jo YH, Sung KR, Shin JW. Peripapillary and macular vessel density measurement by optical coherence tomog-

raphy angiography in pseudoexfoliation and primary open-angle glaucoma. J Glaucoma. 2020;29(5):381–5.
Kashani AH, Chen CL, Gahm JK, et al. Optical coherence tomography angiography: A comprehensive review of current methods and clinical applications. Prog Retin Eye Res. 2017;60:66–100.
Kim M, Kim TW, Weinreb RN, Lee EJ. Differentiation of parapapillary atrophy using spectral-domain optical coherence tomography. Ophthalmology. 2013;120(9):1790–7.
Kim SB, Lee EJ, Han JC, Kee C. Comparison of peripapillary vessel density between preperimetric and perimetric glaucoma evaluated by OCT-angiography. PLoS One. 2017;12(8):e0184297.
Kim JA, Kim TW, Lee EJ, Girard MJA, Mari JM. Microvascular changes in peripapillary and optic nerve head tissues after trabeculectomy in primary open-angle glaucoma. Invest Ophthalmol Vis Sci. 2018;59(11):4614–21.
Kim GN, Lee EJ, Kim H, Kim TW. Dynamic range of the peripapillary retinal vessel density for detecting glaucomatous visual field damage. Ophthalmol Glaucoma. 2019a;2:103–10.
Kim JA, Kim TW, Lee EJ, Girard MJA, Mari JM. Relationship between lamina cribrosa curvature and the microvasculature in treatment-naive eyes. Br J Ophthalmol. 2019b. https://doi.org/10.1136/bjophthalmol-2019-313996.
Kim JS, Kim YK, Baek SU, et al. Topographic correlation between macular superficial microvessel density and ganglion cell-inner plexiform layer thickness in glaucoma-suspect and early normal-tension glaucoma. Br J Ophthalmol. 2020a;104(1):104–9.
Kim GN, Lee EJ, Kim TW. Parapapillary choroidal microvasculature dropout in nonglaucomatous healthy eyes. Acta Ophthalmol. 2020b;98(6):e754–e60.
Kim GN, Lee EJ, Kim TW. Microstructure of nonjuxtapapillary microvasculature dropout in healthy myopic eyes. Invest Ophthalmol Vis Sci. 2020c;61(2):36.
Kumar RS, Anegondi N, Chandapura RS, et al. Discriminant function of optical coherence tomography angiography to determine disease severity in glaucoma. Invest Ophthalmol Vis Sci. 2016;57(14):6079–88.
Kwon J, Choi J, Shin JW, Lee J, Kook MS. Glaucoma diagnostic capabilities of foveal avascular zone parameters using optical coherence tomography angiography according to visual field defect location. J Glaucoma. 2017a;26(12):1120–9.
Kwon J, Choi J, Shin JW, Lee J, Kook MS. Alterations of the foveal avascular zone measured by optical coherence tomography angiography in glaucoma patients with central visual field defects. Invest Ophthalmol Vis Sci. 2017b;58(3):1637–45.
Kwon J, Shin JW, Lee J, Kook MS. Choroidal microvasculature dropout Ii associated with parafoveal visual field defects in glaucoma. Am J Ophthalmol. 2018;188:141–54.
Kwon JM, Weinreb RN, Zangwill LM, Suh MH. Parapapillary deep-layer microvasculature dropout and visual field progression in glaucoma. Am J Ophthalmol. 2019;200:65–75.
Laatikainen L. Fluorescein angiographic studies of the peripapillary and perilimbal regions in simple, capsular and low-tension glaucoma. Acta Ophthalmol Suppl. 1971;111:3–83.
Lee EJ, Kim TW, Weinreb RN. Reversal of lamina cribrosa displacement and thickness after trabeculectomy in glaucoma. Ophthalmology. 2012;119(7):1359–66.
Lee EJ, Lee KM, Lee SH, Kim TW. OCT angiography of the peripapillary retina in primary open-angle glaucoma. Invest Ophthalmol Vis Sci. 2016a;57(14):6265–70.
Lee SH, Yu DA, Kim TW, Lee EJ, Girard MJ, Mari JM. Reduction of the lamina cribrosa curvature after trabeculectomy in glaucoma. Invest Ophthalmol Vis Sci. 2016b;57(11):5006–14.
Lee EJ, Lee SH, Kim JA, Kim TW. Parapapillary deep-layer microvasculature dropout in glaucoma: topographic association with glaucomatous damage. Invest Ophthalmol Vis Sci. 2017a;58(7):3004–10.
Lee EJ, Lee KM, Lee SH, Kim TW. Parapapillary choroidal microvasculature dropout in glaucoma: a comparison between optical coherence tomography angiography and indocyanine green angiography. Ophthalmology. 2017b;124(8):1209–17.
Lee EJ, Kim TW, Lee SH, Kim JA. Underlying microstructure of parapapillary deep-layer capillary dropout identified by optical coherence tomography angiography. Invest Ophthalmol Vis Sci. 2017c;58(3):1621–7.
Lee EJ, Kim TW, Kim JA, Kim JA. Parapapillary deep-layer microvasculature dropout in primary open-angle glaucoma eyes with a parapapillary gamma-zone. Invest Ophthalmol Vis Sci. 2017d;58(13):5673–80.
Lee EJ, Kim TW, Kim JA, Kim JA. Central visual field damage and parapapillary choroidal microvasculature dropout in primary open-angle glaucoma. Ophthalmology. 2018;125(4):588–96.
Lee EJ, Kim TW, Kim JA, et al. Elucidation of the strongest factors influencing rapid retinal nerve fiber layer thinning in glaucoma. Invest Ophthalmol Vis Sci. 2019;60(10):3343–51.
Lee SH, Lee EJ, Kim TW. Comparison of vascular-function and structure-function correlations in glaucomatous eyes with high myopia. Br J Ophthalmol. 2020a;104(6):807–12.
Lee K, Maeng KJ, Kim JY, et al. Diagnostic ability of vessel density measured by spectral-domain optical coherence tomography angiography for glaucoma in patients with high myopia. Sci Rep. 2020b;10(1):3027.
Lee EJ, Kim JA, Kim TW. Influence of choroidal microvasculature dropout on the rate of glaucomatous progression, a prospective study. Ophthalmol Glaucoma. 2020c;3(1):25–31.
Lee EJ, Kim JA, Kim TW, Kim H, Yang HK, Hwang JM. Glaucoma-like parapapillary choroidal microvasculature dropout in patients with compressive optic neuropathy. Ophthalmology. 2020d;127(12):1652–62.
Leske MC, Connell AM, Wu SY, Hyman LG, Schachat AP. Risk factors for open-angle glau-

coma. The Barbados Eye Study. Arch Ophthalmol. 1995;113(7):918–24.
Li XX, Wu W, Zhou H, et al. A quantitative comparison of five optical coherence tomography angiography systems in clinical performance. Int J Ophthalmol. 2018;11(11):1784–95.
Liu L, Jia Y, Takusagawa HL, et al. Optical coherence tomography angiography of the peripapillary retina in glaucoma. JAMA Ophthalmol. 2015;133(9):1045–52.
Liu L, Edmunds B, Takusagawa HL, et al. Projection-resolved optical coherence tomography angiography of the peripapillary retina in glaucoma. Am J Ophthalmol. 2019;207:99–109.
Lommatzsch C, Rothaus K, Koch JM, Heinz C, Grisanti S. OCTA vessel density changes in the macular zone in glaucomatous eyes. Graefes Arch Clin Exp Ophthalmol. 2018;256(8):1499–508.
Lu P, Xiao H, Chen H, Ye D, Huang J. Asymmetry of macular vessel density in bilateral early open-angle glaucoma with unilateral central 10-2 visual field loss. J Glaucoma. 2020;29(10):926–31.
Moghimi S, Zangwill LM, Penteado RC, et al. Macular and optic nerve head vessel density and progressive retinal nerve fiber layer loss in glaucoma. Ophthalmology. 2018;125(11):1720–8.
Moghimi S, Bowd C, Zangwill LM, et al. Measurement floors and dynamic ranges of OCT and OCT angiography in glaucoma. Ophthalmology. 2019;126(7):980–8.
Mursch-Edlmayr AS, Waser K, Podkowinski D, Bolz M. Differences in swept-source OCT angiography of the macular capillary network in high tension and normal tension glaucoma. Curr Eye Res. 2020;45(9):1168–72.
Na HM, Lee EJ, Lee SH, Kim TW. Evaluation of peripapillary choroidal microvasculature to detect glaucomatous damage in eyes with high myopia. J Glaucoma. 2020;29(1):39–45.
Numa S, Akagi T, Uji A, et al. Visualization of the lamina cribrosa microvasculature in normal and glaucomatous eyes: a swept-source optical coherence tomography angiography study. J Glaucoma. 2018;27(11):1032–5.
O'Brart DP, de Souza LM, Bartsch DU, Freeman W, Weinreb RN. Indocyanine green angiography of the peripapillary region in glaucomatous eyes by confocal scanning laser ophthalmoscopy. Am J Ophthalmol. 1997;123(5):657–66.
Park SC, De Moraes CG, Teng CC, Tello C, Liebmann JM, Ritch R. Initial parafoveal versus peripheral scotomas in glaucoma: risk factors and visual field characteristics. Ophthalmology. 2011;118(9):1782–9.
Park HY, Shin DY, Jeon SJ, Park CK. Association between parapapillary choroidal vessel density measured with optical coherence tomography angiography and future visual field progression in patients with glaucoma. JAMA Ophthalmol. 2019;137(6):681–8.
Philip S, Najafi A, Tantraworasin A, Chui TYP, Rosen RB, Ritch R. Macula vessel density and foveal avascular zone parameters in exfoliation glaucoma compared to primary open-angle glaucoma. Invest Ophthalmol Vis Sci. 2019;60(4):1244–53.
Rao HL, Pradhan ZS, Weinreb RN, et al. A comparison of the diagnostic ability of vessel density and structural measurements of optical coherence tomography in primary open angle glaucoma. PLoS One. 2017a;12(3):e0173930.
Rao HL, Kadambi SV, Weinreb RN, et al. Diagnostic ability of peripapillary vessel density measurements of optical coherence tomography angiography in primary open-angle and angle-closure glaucoma. Br J Ophthalmol. 2017b;101(8):1066–70.
Rolle T, Dallorto L, Tavassoli M, Nuzzi R. Diagnostic ability and discriminant values of OCT-angiography parameters in early glaucoma diagnosis. Ophthalmic Res. 2019;61(3):143–52.
Schwartz B, Rieser JC, Fishbein SL. Fluorescein angiographic defects of the optic disc in glaucoma. Arch Ophthalmol. 1977;95(11):1961–74.
Sehi M, Goharian I, Konduru R, et al. Retinal blood flow in glaucomatous eyes with single-hemifield damage. Ophthalmology. 2014;121(3):750–8.
Shiga Y, Kunikata H, Aizawa N, et al. Optic nerve head blood flow, as measured by laser speckle flowgraphy, is significantly reduced in preperimetric glaucoma. Curr Eye Res. 2016;1–7.
Shin JW, Lee J, Kwon J, Choi J, Kook MS. Regional vascular density-visual field sensitivity relationship in glaucoma according to disease severity. Br J Ophthalmol. 2017a;101(12):1666–72.
Shin JW, Sung KR, Uhm KB, et al. Peripapillary microvascular improvement and lamina cribrosa depth reduction after trabeculectomy in primary open-angle glaucoma. Invest Ophthalmol Vis Sci. 2017b;58(13):5993–9.
Shin JW, Kwon J, Lee J, Kook MS. Choroidal microvasculature dropout is not associated with myopia, but is associated with glaucoma. J Glaucoma. 2018;27(2):189–96.
Shin JW, Kwon J, Lee J, Kook MS. Relationship between vessel density and visual field sensitivity in glaucomatous eyes with high myopia. Br J Ophthalmol. 2019;103:585–91.
Simsek M, Kocer AM, Cevik S, Sen E, Elgin U. Evaluation of the optic nerve head vessel density in the patients with asymmetric pseudoexfoliative glaucoma: an OCT angiography study. Graefes Arch Clin Exp Ophthalmol. 2020;258(7):1493–501.
Spaide RF, Klancnik JM Jr, Cooney MJ. Retinal vascular layers imaged by fluorescein angiography and optical coherence tomography angiography. JAMA Ophthalmol. 2015a;133(1):45–50.
Spaide RF, Fujimoto JG, Waheed NK. Image artifacts in optical coherence tomography angiography. Retina. 2015b;35(11):2163–80.
Suh MH, Zangwill LM, Manalastas PI, et al. Deep retinal layer microvasculature dropout detected by the optical coherence tomography angiography in glaucoma. Ophthalmology. 2016;123(12):2509–18.
Suh MH, Park JW, Kim HR. Association between the deep-layer microvasculature dropout and the visual field damage in glaucoma. J Glaucoma. 2018;27(6):543–51.

Takusagawa HL, Liu L, Ma KN, et al. Projection-resolved optical coherence tomography angiography of macular retinal circulation in glaucoma. Ophthalmology. 2017;124(11):1589–99.

Tielsch JM, Katz J, Sommer A, Quigley HA, Javitt JC. Hypertension, perfusion pressure, and primary open-angle glaucoma. A population-based assessment. Arch Ophthalmol. 1995;113(2):216–21.

Venugopal JP, Rao HL, Weinreb RN, et al. Repeatability of vessel density measurements of optical coherence tomography angiography in normal and glaucoma eyes. Br J Ophthalmol. 2018;102(3):352–7.

Wang RK. Optical microangiography: a label free 3D imaging technology to visualize and quantify blood circulations within tissue beds in vivo. IEEE J Sel Top Quantum Electron. 2010;16(3):545–54.

Wu J, Sebastian RT, Chu CJ, McGregor F, Dick AD, Liu L. Reduced macular vessel density and capillary perfusion in glaucoma detected using OCT angiography. Curr Eye Res. 2019;44(5):533–40.

Xu H, Zhai R, Zong Y, et al. Comparison of retinal microvascular changes in eyes with high-tension glaucoma or normal-tension glaucoma: a quantitative optic coherence tomography angiographic study. Graefes Arch Clin Exp Ophthalmol. 2018;256(6):1179–86.

Yamazaki S, Inoue Y, Yoshikawa K. Peripapillary fluorescein angiographic findings in primary open angle glaucoma. Br J Ophthalmol. 1996;80(9):812–7.

Yarmohammadi A, Zangwill LM, Diniz-Filho A, et al. Relationship between optical coherence tomography angiography vessel density and severity of visual field loss in glaucoma. Ophthalmology. 2016;123(12):2498–508.

Yarmohammadi A, Zangwill LM, Manalastas PIC, et al. Peripapillary and macular vessel density in patients with primary open-angle glaucoma and unilateral visual field loss. Ophthalmology. 2018;125(4):578–87.

Yoo E, Yoo C, Lee TE, Kim YY. Comparison of retinal vessel diameter between open-angle glaucoma patients with initial parafoveal scotoma and peripheral nasal step. Am J Ophthalmol. 2017;175:30–6.

Zhang X, Beckmann L, Miller DA, et al. In vivo imaging of Schlemm's canal and limbal vascular network in mouse using visible-light OCT. Invest Ophthalmol Vis Sci. 2020;61(2):23.

Zivkovic M, Dayanir V, Kocaturk T, et al. Foveal avascular zone in normal tension glaucoma measured by optical coherence tomography angiography. Biomed Res Int. 2017;2017:3079141.